Accepted Article Preview: Published ahead of advance online publication

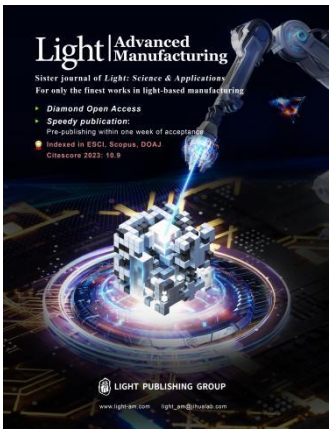

Directional Leidenfrost Droplet Propulsion on Femtosecond-Laser-Engineered Dual Heterogeneous Surfaces with Hybrid Boiling States

Dong Wu, Cunyuan Chen, Keyi Zhang, Mingyang Wang, Zhixiang Zhao, Zhenrui Chen, Xinlei Li, Hao Wu, Youdi Hu, Suwan Zhu, Yanlei Hu, Chaowei Wang, and Jiale Yong

Cite this article as: Dong Wu, Cunyuan Chen, Keyi Zhang, Mingyang Wang, Zhixiang Zhao, Zhenrui Chen, Xinlei Li, Hao Wu, Youdi Hu, Suwan Zhu, Yanlei Hu, Chaowei Wang, Jiale Yong. Directional Leidenfrost Droplet Propulsion on Femtosecond-Laser-Engineered Dual Heterogeneous Surfaces with Hybrid Boiling States. *Light: Advanced Manufacturing* accepted article preview 17 April, 2026; doi: 10.37188/lam.2026.068

Received 03 September 2025; revised 10 April 2026; accepted 16 April 2026; Accepted article preview online 17 April 2026

Directional Leidenfrost Droplet Propulsion on Femtosecond-Laser-Engineered Dual Heterogeneous Surfaces with Hybrid Boiling States

Dong Wu,[1] Cunyuan Chen,[1] Keyi Zhang,[2] Mingyang Wang,[2] Zhixiang Zhao,[3] Zhenrui Chen,[1] Xinlei Li,[1] Hao Wu,[1] Youdi Hu,[1] Suwan Zhu,[4] Yanlei Hu,[1] Chaowei Wang,[1,] and Jiale Yong[1,*]*

[1]State Key Laboratory of Opto-Electronic Information Acquisition and Protection, Key Laboratory of Precision Scientific Instrumentation of Anhui Higher Education Institutes, Department of Precision Machinery and Precision Instrumentation, University of Science and Technology of China, Hefei, 230027, China

[2]Intelligent Manufacturing Laboratory, School of Mechanical and Electrical Engineering, Anhui Jianzhu University, Hefei, 230009, China

[3]School of Urban Planning and Municipal Engineering, Xi'an Polytechnic University, Xi'an, 710048, China

[4]Department of Optical Engineering, School of Physics, Hefei University of Technology, Hefei 230601, China

*Corresponding author: jlyong@ustc.edu.cn (J.Y.), chaoweiw@ustc.edu.cn (C.W.)

Abstract

Liquid propulsion on overheated surfaces plays an important role in numerous engineering applications. However, most reported methods are limited to homogeneous asymmetric structures such as ratchet-shaped substrates. In this study, a dual heterogeneous structure is designed on an aluminium surface via femtosecond laser direct writing. The substrate surface is alternately covered with non-ablated smooth strips and laser-structured regions composed of periodic ripple microstructures. The droplets on the heated sheet exhibit a hybrid boiling state: film boiling in the smooth regions and intermittent transition boiling in the ripple microstructures. This hybrid state enables the droplets to remain in the Leidenfrost regime and combines the advantages of both the film- and transition-boiling states. That is, droplets on hot surfaces combine the long lifetime characteristic of the film-boiling state with the efficient substrate–liquid heat exchange of the contact-boiling state, achieving a balance between extended lifespan and effective heat transfer. The film-boiling regions facilitate the formation of a stable vapour cushion beneath the droplet, whereas the intermittent asymmetric contact boiling on

the ripple microstructures produces a directional driving force and unidirectionally propels the Leidenfrost droplets. In particular, the droplets consistently move along the laser-scanning lines and opposite the laser processing direction. By ingeniously designing laser processing paths, diverse functions and applications of Leidenfrost droplet propulsion, including curved-path droplet transport, droplet expulsion, droplet trapping, targeted cooling, and droplet rotors, can be realised.

Keywords: Leidenfrost droplet, femtosecond laser writing, directional propulsion, ripple microstructure, Leidenfrost effect

1. Introduction

When droplets are poured onto an overheated solid surface whose temperature is far above the boiling point of the liquid, the droplets do not evaporate quickly or splash violently but are instead suspended over the hot substrate. This interesting physical phenomenon is known as the 'Leidenfrost effect'.[1-5] A downward jet of vapour, caused by the thermally induced phase transition at the bottom of the droplets, lifts the droplets and allows them to levitate above the solid surface. The vapour layer has poor thermal conductivity, which can effectively inhibit heat transfer between the hot surface and the droplet.[6-8] The vapour layer separates the droplet from the solid substrate, thus reducing droplet adhesion and eliminating the associated interfacial friction.[9-11] These two characteristics make the Leidenfrost effect widely applicable in metal processing and welding, low-friction sliding systems, cooling systems, chemical engineering, microfluidic technology, and energy conversion.[1,3,12-18] The application of the Leidenfrost effect not only improves the efficiency and quality of industrial production but also reduces safety risks.

Because many applications depend on the high-speed propulsion of Leidenfrost droplets, the controllable transport of Leidenfrost droplets on overheated surfaces has attracted increasing interest over the past two decades.[1,3,19,20] Linke *et al.* found that Leidenfrost droplets can directionally self-propel on a hot sawtooth-shaped substrate composed of periodic millimetre-scale ratchets.[21,22] The high temperature causes the liquid at the bottom of the droplet to evaporate quickly and spray the vapour downward. The surface of the asymmetric ratchets could partially rectify the flow direction of the steam, thereby creating a viscous shear stress at the bottom of the droplet, which directionally pushes the suspended Leidenfrost droplet into motion. Several other types of asymmetric structures have been designed to achieve directional transport of Leidenfrost droplets, including slanted superhydrophilic silicon nanowires,[23] triangular micropillar arrays,[24] herringbone patterns,[25,26]

angled mound-like microstructures,[27] periodic wettability gradients,[28,29] and hot oil surfaces.[30] These microstructures are typically fabricated uniformly on the material surface, causing droplets on the heated surface to exist either in the contact-boiling state (*e.g.,* transition boiling) or film-boiling state.[1-5] For droplets in the transition-boiling state, despite the high heat-transfer efficiency from the substrate to the droplet, violent and persistent contact boiling makes droplet motion uncontrollable, often causing the droplets to move randomly on the hot surface.[31,32] Additionally, vigorous boiling and spraying at the contact interface significantly shortens the droplet lifespan. In contrast, droplets in the film-boiling state exhibit 'gentle' and more controllable behaviour due to the vapour layer beneath them, along with a longer lifespan.[2,4] However, this vapour layer also isolates the bottom of the droplet from direct contact with the hot solid surface, limiting efficient energy (*e.g.,* thermal energy) transfer between the heated substrate and the droplets.[6] High heat-transfer resistance is detrimental to effective thermal management.[29,31] A single boiling state can provide only the advantages associated with that state while failing to overcome its inherent limitations. For example, a droplet in the film-boiling regime, although exhibiting the longest lifetime on an overheated surface, suffers from a relatively low heat-transfer efficiency, whereas in the contact-boiling regime, despite the extremely high heat-transfer efficiency between the heated surface and the liquid, the droplet tends to splash and disintegrate almost instantaneously. Integration of multiple boiling states can effectively leverage the strength of each state. Under the premise of balancing droplet lifetime and heat-transfer efficiency, achieving the controllable motion of Leidenfrost droplets is of great significance for practical applications. However, the dynamic behaviour of droplets in a hybrid boiling state (such as on heterogeneously structured surfaces) under high-temperature conditions has received relatively sparse attention.[33] Sahoo *et al.* observed a Janus thermal state (concurrent contact boiling and Leidenfrost effect) on an overheated surface composed of alternating hydrophilic SiN tops and V-shaped Si microgrooves.[34] In this configuration, while the bottom of the droplet undergoes contact boiling on the SiN ridge tops, it experiences film contact over the microgrooves. Despite the anisotropic, elongated bouncing of the water droplet after impacting the hot surface, the position of the droplet remains unchanged, indicating that no directional transport is induced.

In this study, we fabricated a dual heterogeneous structure on aluminium surfaces via femtosecond laser direct writing and discovered unidirectional self-propulsion of droplets in the approximate Leidenfrost state. The alternating pattern of the laser-structured and non-ablated smooth regions allows droplets on the heated surface to exhibit film boiling and transition boiling regimes simultaneously. This hybrid state causes the droplets to remain in the Leidenfrost regime on the heated substrate, achieving a balance between extended lifespan and effective heat transfer. The

laser-induced periodic asymmetric ripple microstructures enabled intermittent contact with the bottom of the droplet, resulting in asymmetric contact boiling at localised hot spots and driving the directional motion of the droplets. Specifically, the droplets move exclusively along the laser-scanning paths, precisely opposite to the laser processing direction. By leveraging this characteristic, the controllable propulsion of Leidenfrost droplets can be easily achieved by designing specific laser-scanning trajectories, enabling various droplet manipulation functions and applications on heated surfaces.

2. Results and Discussion

2.1 Unidirectional droplet propulsion

Figure 1a illustrates the femtosecond laser processing of the aluminium surface and the motion trend of water droplets on the heated surface. Femtosecond laser machining is characterised by high accuracy, excellent controllability, and broad material compatibility.[35-38] The direction of the laser-scanning line is defined as the +x-axis; the direction perpendicular to the laser-scanning line on the horizontal plane is the y-axis; and the direction perpendicular to the horizontal plane is the z-axis. The laser processing system is depicted in Figure S1 (Supporting Information). The employed femtosecond laser beam was a pulsed laser with a repetition rate (f_{rep}) of 1 kHz and was focused on the sample surface through an F-theta lens, with a spot diameter of ≈30 μm. Each pulse can induce a concave crater-like microstructure on the sample surface.

The positional relationship between the craters along a scanning line can be easily adjusted by changing the laser-scanning speed (V_{laser}). As shown in Figure 1b, when the laser-scanning speed is sufficiently high, the laser pulse-induced craters separate from each other. As the laser-scanning speed decreases, the distance between the ablated points of the pulses as well as the period ($\Lambda_{crater} = V_{laser} \times \frac{1}{f_{rep}}$) of the laser-induced craters decreases. When the spacing between the laser processing points is less than the diameter (D_{crater}) of a single crater, the laser-induced craters overlap. The next laser-induced crater is superimposed on top of the former crater. When the laser-scanning speed is particularly low, the ablation craters strongly overlap.

Figures 1c–f show the crater array microstructure (or microgroove structure) fabricated on the aluminium surface at different laser-scanning speeds. When the laser-scanning speed is 60 mm/s, the ablation craters are separated from each other at a corresponding interval of 60 μm (Figure 1c). Every crater is complete and has a

diameter of ≈53 μm, obtained at a single-pulse power of 350 μJ. Because only a single pulse acts on each spot without pulse overlap, the ablation craters are relatively shallow, with a depth of only ≈2.5 μm. When the scanning speed is reduced to 40 mm/s, the ablation craters begin to overlap (Figure 1d). The overlap ratio (η) can be defined as $\eta = \frac{D_{crater} - \Lambda_{crater}}{D_{crater}} \times 100\%$ (when $\Lambda_{crater} \leq D_{crater}$). With this processing parameter, the craters slightly overlap, with a η of 24.5%. When the scanning speed is further reduced to 30 mm/s (η = 43.4%), the next crater almost overlaps half of the previous crater, eventually forming a wavy ripple-like microstructure along the laser-scanning direction, defined here as the 'ripple microstructure', as shown in Figure 1e. When the laser-scanning speed is as low as 10 mm/s, owing to the high degree of crater overlap (η = 81.1%), the ripple-like microstructures disappear and are replaced by a uniformly rough microgroove (Figure 1f). The average distance of the craters or the microgrooves along the *y* direction is controlled by the interval (Λ_{line}) of the scanning lines during laser processing.

Femtosecond laser treatment also altered the surface wettability of the aluminium substrate. The surface becomes more hydrophilic as it is covered with more laser-induced micro/nanostructures. For example, as shown in Figure S2 and Movie S1 (Supporting Information), the contact angle (CA) of a water droplet decreases from 100.3 ± 0.9° on the original unstructured aluminium surface to 5.4 ± 1.2° (Λ_{crater} = 30 μm, Λ_{line} = 100 μm) and 6.3 ± 0.6° (Λ_{crater} = 30 μm, Λ_{line} = 60 μm) on the laser-structured surfaces. In addition, the laser-induced microstructures also raise the critical Leidenfrost temperature of water droplets on the aluminium sheet from ≈200 ℃ on the untreated smooth surface to over 600 ℃.

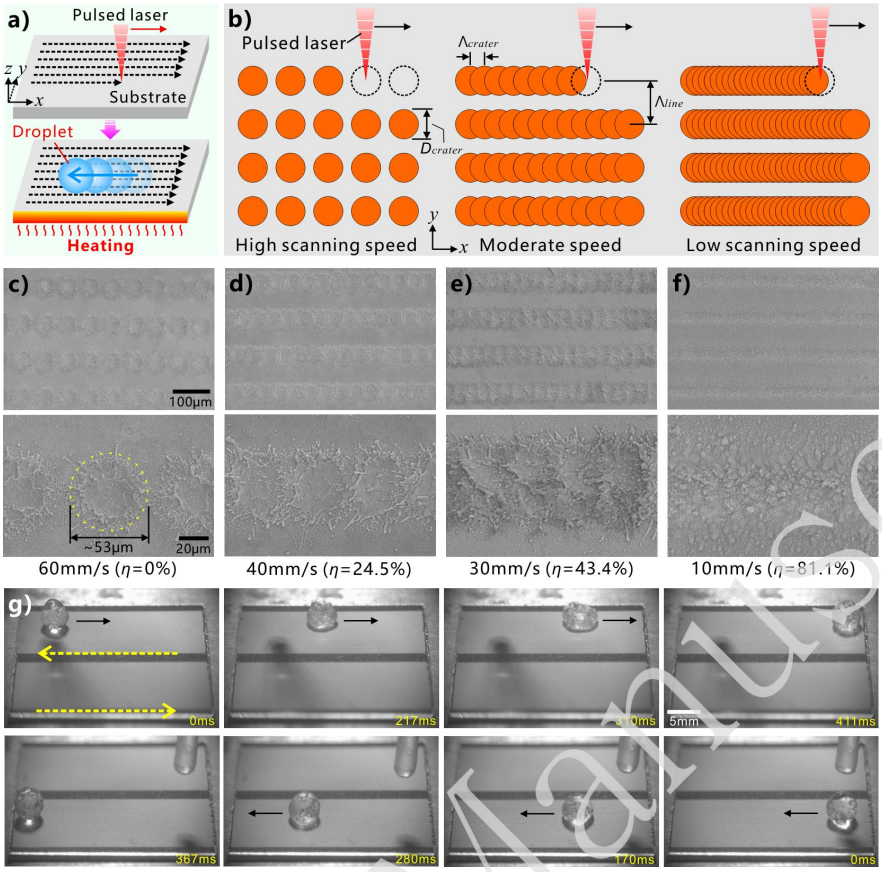

Figure 1. Unidirectional propulsion of Leidenfrost droplets on the femtosecond laser-structured heterogeneous aluminium surface. (a) Schematic showing the manner of laser processing of the aluminium surface and the motion trend of water droplets on the heated laser-structured sheet. (b) Schematic illustrating different positional relationships between the laser pulse-induced craters (or pits). (c-f) Laser-induced microstructures on the aluminium surface prepared at different laser-scanning speeds (Λ_{line} = 100 μm): (c) V_{laser} = 60 mm/s, (d) V_{laser} = 40 mm/s with an η of 24.5%, (e) V_{laser} = 30 mm/s with an η of 43.4%, and (f) V_{laser} = 10 mm/s with an η of 81.1%. (g) Motion trajectory of droplets on a heated structured aluminium sheet (250 °C, η = 43.4%, Λ_{line} = 100 μm) where the upper half region was processed via laser scanning from right to left and the lower half region was processed from left to right. The yellow dashed arrows mark the laser processing direction, while the black solid arrows indicate the droplet's movement direction.

On a heated laser-structured surface, the droplet can be self-driven along the laser-scanning lines (Figure 1a). As shown in Figure 1g, we use a femtosecond laser to process two regions (η = 43.4%, Λ_{line} = 100 μm) on the same surface of an aluminium sheet (thickness = 1 mm). The laser processing directions are opposite in these two regions. At a heating temperature of 250 °C, when the droplets (≈50 μL) are dropped onto the upper region, where the laser-scanning lines are processed from right to left (yellow dotted arrow), the droplets spontaneously move towards the right at a high speed on the heated substrate (Movie S2, Supporting Information). During the advancing process, the droplet can maintain a nearly spherical shape on the heated

surface, similar to the behaviour of a small water droplet on a superhydrophobic surface. This characteristic is typical of Leidenfrost droplets and indicates that on the heated surface, the droplet moves in a state approaching the Leidenfrost regime.[1,5] In contrast, in the lower region, where the laser-scanning lines are processed from left to right, the deposited droplets move to the left instead (Movie S2, Supporting Information). The design of two structured regions, with opposite processing directions, on the same aluminium sheet can eliminate the influence of gravity on the results (even a small force component of gravity can cause the droplet motion because the adhesion of the heated surface to the Leidenfrost droplets is extremely low).[28] The results indicate that femtosecond-laser-induced ripple microstructures can unidirectionally drive the movement of droplets on a hot surface and that the propulsion direction is opposite to that of laser processing.

2.2 Influence of various parameters on the droplet propulsion

On a smooth aluminium surface (without laser treatment), water droplets deposited onto a heated surface successively exhibit natural evaporation, nucleate boiling, transition boiling, and film-boiling states as the heating temperature gradually increases. The detailed dynamic behaviour of droplets in these regimes has been extensively reported in the literature and can also be found in our previous work.[1,4,5,32,34] Figures 2a–d and Movie S3 (Supporting Information) show the variation in the dynamic behaviour of the water droplets on the laser-structured heterogeneous surface (η = 43.4%, Λ_{line} = 100 μm) as the heating temperature gradually increases. When the temperature of the aluminium substrate is just above the boiling point (≈100 ℃) of water, the droplets still slowly evaporate on the textured surface (*e.g.,* at 120 ℃, Figure 2a). As the heating temperature increases above 160 ℃, the droplets enter a state of nuclear boiling. Once the droplets touch the hot surface, they violently boil, burst, and splash around (*e.g.,* at 200 ℃, Figure 2b). The droplets disappeared in a very short time (≈770 ms) because of intense spraying and rapid evaporation. When the temperature exceeds a certain threshold (230 ℃ for this structure), the droplets can maintain a spherical shape on the heated surface without explosion or fragmentation. Interestingly, the droplets begin to move rapidly on the surface, and the direction of motion is fixed (*e.g.*, at 260 ℃, Figure 2c). Thus, unidirectional propulsion of liquid droplets is realised. During the movement of the droplet, a thin transparent layer (inset of Figure 2c) between the bottom of the droplet and the solid surface can be clearly observed, which is attributed to the vapour layer underneath the heated droplet. The existence of a stable vapour layer provides visual evidence of the Leidenfrost state. However, the temperature should not be excessively high. When the surface temperature increases to 280 ℃ (*i.e.,* the upper threshold for this structure), the droplet continues to advance forward while deflecting towards both

sides in the forward direction. The lateral deflection indicates that the directional droplet propulsion at this temperature is already extremely weak. Upon further increasing the substrate temperature, the directional motion completely disappears. For example, at 290 °C, the droplet in the captured snapshots gradually becomes blurred because it moves in a direction (*y*-axis) perpendicular to the image (Figure 2d). At this instance, although the droplets can still move on a heated surface, the direction of movement is random; that is, no directional propulsion occurs.

In addition to water, a variety of other volatile liquids can achieve directional transport on heat-structured surfaces as long as the heating temperature falls within the appropriate range for each specific liquid. As shown in Figure S3 and Movie S4 (Supporting Information), the laser-induced microstructures can drive droplets of ethylene glycol, propylene glycol, 50% ethanol, anhydrous ethanol, and acetone to move directionally at high speeds. Furthermore, the direction of movement of these droplets is consistent with that of the water droplets. These liquids exhibit varying physicochemical properties.[39]

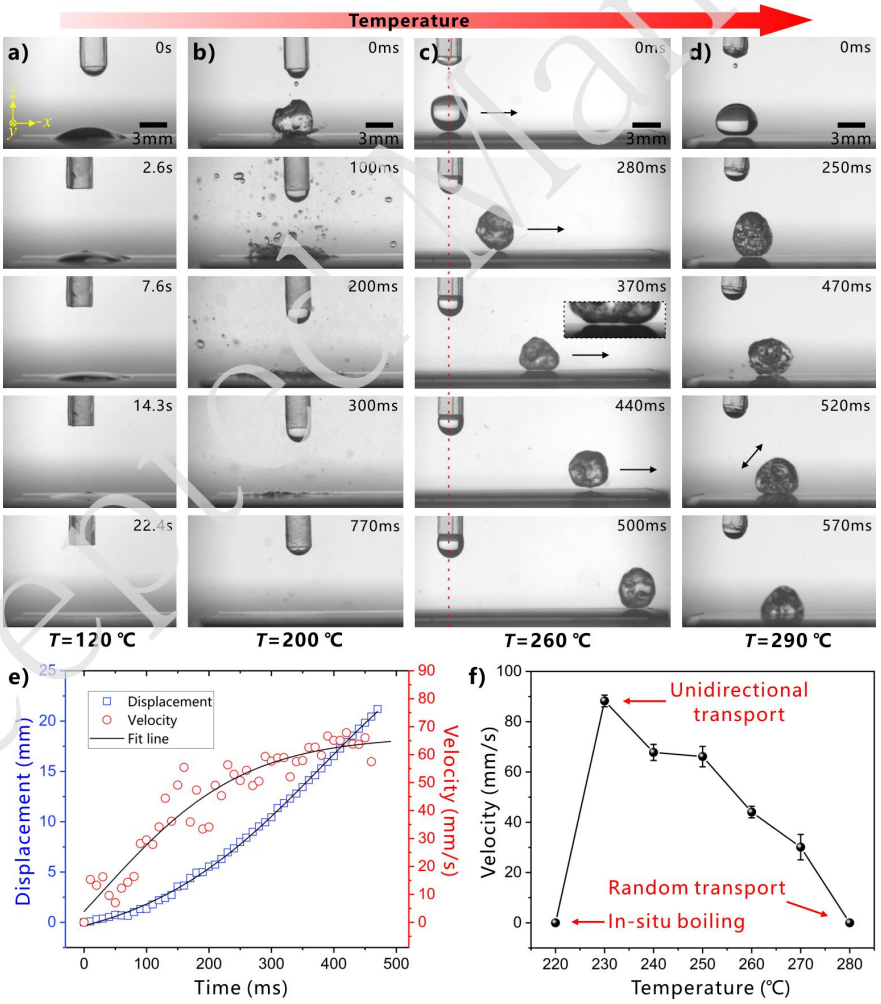

Figure 2. Unidirectional transport of droplets (≈50 µL) on heated aluminium sheets with femtosecond laser-written ripple microstructures (V_{laser} = 30 mm/s, Λ_{line} = 100 µm). (a–d) Influence of the heating temperature on the dynamic behaviour of the deposited droplets on the structured aluminium surface: (a) slow evaporation at 120 °C,

(b) in-situ nuclear boiling at 200 °C, (c) directional propulsion at 260 °C, and (d) random motion at 290 °C. The inset in (c) is an enlarged view of the interface between the droplet and the solid substrate, showing the existence of a vapour layer between the droplet bottom and the hot surface. (e) Variation in the displacement and motion velocity of the droplet over time on the heated aluminium surface (at 250 °C). (f) Terminal velocity (or maximum motion velocity) of droplets on the heated surface at different heating temperatures.

During the motion, the suspended droplet is subjected to the resistance of the surrounding air in addition to the driving force (F_d). Owing to the low Reynolds number (≈0.2) of the Leidenfrost droplets, according to Stokes' friction law, the air resistance force (F_r) is linearly related to the droplet velocity: $F_r \sim -k_f v_x(t)$, where $v_x(t)$ is the horizontal velocity of the droplet, t is time, and k_f is the friction coefficient.[21,40,41] According to Newton's second law, the velocity of a droplet satisfies the following ordinary differential equation: $M\frac{dv_x(t)}{dt} = F_d - \sigma k_f v_x(t)$, where M is the mass of the droplet and σ is the proportion coefficient. The droplets accelerate continuously on the heated structured surface. At $\frac{dv_x(t)}{dt} = 0$, the velocity of the droplet reaches its maximum value (*i.e.*, the terminal velocity): $v_t = \frac{F_d}{\sigma k_f}$.

Figure 2e shows the horizontal displacement and motion velocity of the droplet in the process of unidirectional propulsion over time (at 250 °C). The horizontal displacement of the droplet from the point at which it is deposited on the sample surface increases gradually. The velocity of the droplet first increases and finally approaches a stable value. The maximum velocity can reach ≈65 mm/s, and the test results are in agreement with those of the theoretical analysis. Figure 2f shows the effect of the heating temperature on the terminal velocity achievable by the droplets on the structured surface. As the temperature increases, the maximum velocity of the droplets gradually decreases from 88.3 ± 2.3 (at 230 °C) to 30.1 ± 5.1 (at 270 °C) and then to 0 mm/s (at 280 °C, random transport). This trend may occur because higher heating temperatures lead to a thicker vapour layer underneath the droplets (owing to enhanced evaporation), which progressively weakens the influence of the laser-induced ripple microstructures on the dynamic behaviour of the droplets. In other words, the overall height of the droplet bottom increases with increasing temperature, and the driving effect of the laser-induced microstructures on the droplets gradually weakens.

Figures 3a–d show the influence of laser processing and physical parameters of the liquid droplets on the dynamic motion state of the droplets on the structured

aluminium surface. As shown in Figure 3a, when the laser-scanning speed is either extremely low or excessively high, the droplet cannot achieve unidirectional motion. If the V_{laser} is extremely low, then the overlap of single-pulse-ablated craters is relatively heavy (η > 71.7%), resulting in uniform micro/nanostructures rather than asymmetric ripple structures inside the laser-induced microgrooves. Conversely, if the V_{laser} is extremely high, then the craters become separated (η < 15.1%). Only at an appropriate V_{laser} range, corresponding to the overlap ratio range of the laser ablation craters (15.1–71.7%), can periodic asymmetric textures form along the laser-scanning lines, enabling the droplet to move unidirectionally on the heated resulting surface. The interval between the laser-scanning lines also affects the motion of the droplet (Figure 3b). When Λ_{line} is extremely small, the droplet either boils in place at low temperatures or moves randomly at high temperatures, failing to achieve unidirectional propulsion. This result is obtained because the adjacent scanning lines overlap when they are too close, preventing the formation of separate and unbroken microgrooves with the inner periodic craters. Unidirectional droplet motion is only possible when the Λ_{line} is greater than the width of a single laser-induced microgroove (Λ_{line} > 60 μm), within a suitable heating temperature range. However, if the Λ_{line} is too large (*e.g.,* Λ_{line} > 130 μm), unidirectional motion is also difficult to achieve, likely because the groove density is too low (too sparse), resulting in an insufficient directional driving force on the droplet. Within the range of the laser processing parameters that enable directional droplet propulsion, the terminal velocity of the droplets gradually decreases as the laser-scanning speed increases (Figure 3e) or the interval of the scanning lines widens (Figure 3f). This phenomenon occurs because these parameter changes reduce the number of laser-induced craters per unit area (*i.e.,* decreasing the density of craters), thereby progressively diminishing the contribution of the laser-induced ripple microstructures to droplet propulsion.

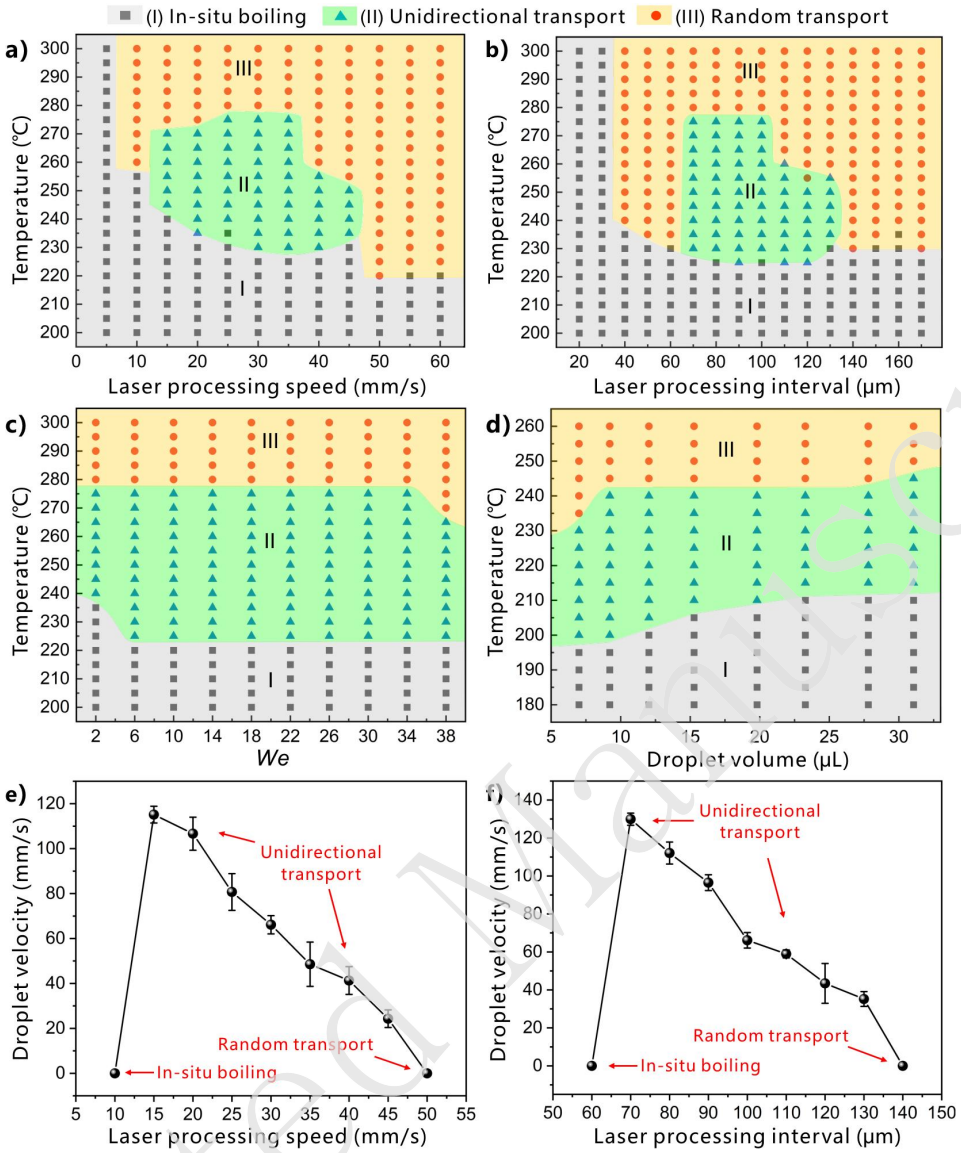

Figure 3. Factors affecting the dynamic behaviour of droplets on heated heterogeneous aluminium surfaces. (a,b) Phase diagrams showing the influence of the laser processing parameters on the droplet motion state: (a) the laser-scanning speed (Λ_{line} = 100 μm) and (b) the interval of the laser-scanning lines (V_{laser} = 30 mm/s). (c,d) Phase diagrams showing the influence of the physical parameters of the droplets on the droplet motion state: (c) Weber number (*We*) and (d) droplet volume (V_{laser} = 30 mm/s, Λ_{line} = 100 μm). (e,f) Influence of (e) the laser-scanning speed and (f) the interval of the scanning lines on the terminal velocity achieved by the droplets on the heated aluminium surfaces (at 250 °C).

By releasing droplets from different heights onto the heated surface, we investigated the influence of the Weber number (*We*) on the dynamic behaviour of the droplets, as shown in Figure 3c. Here, $We = \frac{\rho_l v_0^2 R}{\gamma}$, where ρ_l and γ are the density and surface tension of the liquid, v_0 is the impact velocity, and R is the equatorial radius of the droplet. Regardless of the release height, the droplets uniformly

underwent three states (*i.e.,* in-situ boiling, unidirectional transport, and random motion) as the heating temperature increased from low to high. Moreover, for *We* ranging from 6 to 34, the critical temperature thresholds between these three states remain almost unchanged, indicating that the Weber number (representing the release height of the droplets) negligibly affects the dynamic behaviour of the droplet on the laser-structured heterogeneous surface. Releasing the droplet from an extremely low height (*We* = 2) results in a higher critical temperature for transitioning from the boiling state to the unidirectional transport state, likely because the droplet has not fully detached from the nozzle of the syringe needle when its bottom contacts the heated surface. Conversely, releasing a droplet from a large height (*We* = 38) leads to a lower critical temperature for transitioning from unidirectional transport to a random motion state because the droplet breaks upon impact with the metal surface owing to the excessive impact velocity. Figure 3d shows the effect of the droplet volume (7.0–31.1 μL) on the droplet's state. Similarly, both small and large droplets underwent the same three dynamic processes as the heating temperature increased. As the droplet volume increases, the critical temperature for transitioning from the boiling state to the unidirectional transport state gradually increases, indicating that larger droplets are slightly more difficult to drive directionally. Except for extremely small droplets, the volume negligibly affects the critical temperature for transitioning from the unidirectional transport state to a random motion state.

Furthermore, the superhydrophilicity of the structured sample and its ability to drive Leidenfrost droplets remain highly stable without gradual degradation during heating. As shown in Figure S4a (Supporting Information), even after heating at 260 °C for 7 days (168 h), the structured aluminium surface retains its initial superhydrophilicity, with a CA of ≈0° to water droplets. This contrasts with the behaviour of typical laser-processed metal surfaces, which tend to transition to a superhydrophobic state when exposed to air over time.[42,43] The observed stability may be attributed to two factors. The laser ablation of the aluminium surface in this experiment is relatively mild, resulting in shallow surface structures composed mainly of nanoparticles. Conversely, continuous heating at 260 °C thermally cleans the surface by removing organic adsorption layers that typically induce hydrophobicity, while potentially promoting the regeneration and stabilisation of hydrophilic surface hydroxyl groups through thermal activation. This leads to long-term superhydrophilicity. The stable wetting performance enables the structured surface to effectively drive water droplets onto the heated surface even after seven days of heating, as shown in Figure S4b in the Supporting Information.

2.3 Mechanism of directional droplet propulsion

Figure 4 illustrates the mechanism of directional droplet propulsion on a laser-induced

heterogeneous surface. First, we clarified the dynamic state of a droplet on a heated aluminium surface. As observed in Figure 2c and Movie S3 (Supporting Information), a transparent vapour layer always persists between the moving droplet and the aluminium substrate during the entire motion process. In addition, the droplet maintains an essentially spherical shape despite minor shape fluctuations. These characteristics indicate that the droplet is primarily in the Leidenfrost state.[1,2,4,33] However, the behaviour of the droplet deviates slightly from that of an ideal Leidenfrost droplet. Bubbles form inside the heated droplet on the laser-structured surface, a phenomenon rarely observed in the classical Leidenfrost phenomenon. As shown in Figure S5 and Movie S5 (Supporting Information), when a water droplet first contacts the heated surface, numerous small bubbles with a diameter of approximately 0.14–0.41 mm appear inside the droplet. These bubbles are generated from the contact interface between the water and heated substrate. After the droplet rebounds and falls again, upon its second contact with the hot surface, the number of bubbles inside the droplet decreases, whereas their diameters increase to approximately 0.27–0.84 mm. As the droplet repeatedly contacts the heated surface, the bubble diameter gradually increases, whereas the number of bubbles gradually decreases. Eventually, only a few large bubbles with diameters ranging from 1.17 to 1.89 mm remain stably inside the droplet and move with the motion of the Leidenfrost droplet. As the droplet bounces or oscillates up and down, intermittent contact between the bottom and heated surface leads to a mild ejection of tiny satellite droplets from the two sides of the droplet bottom.

The detailed characteristics of the ejected satellite droplets can be observed directly from the slow-motion playback of the high-speed camera footage, as shown in Figure S6 and Movie S6 (Supporting Information). Small droplet ejection is a characteristic of contact boiling, particularly in the transition-boiling state.[29,32,44] However, the ejections in our experiments are sporadic and far less violent than those in the typical transition-boiling state. Thus, the droplet dynamics on the laser-structured surface exhibit features of both the film-boiling state (Leidenfrost state) and transition-boiling state (contact boiling state), suggesting an intermediate state.[1,2,33] This mixed state may arise from the heterogeneous surface morphology of the heated aluminium substrate (Figure 4a). The laser-written ripple microstructures coexist with the untreated smooth regions, indicating that the aluminium surface comprises both laser-induced ripples and unmodified areas. Taking the heating temperature of 250 °C (exceeding the Leidenfrost temperature of water on a smooth aluminium substrate) as an example, a droplet on the untreated smooth aluminium sheet (without surface microstructures) remains in the Leidenfrost state, stably levitating with a vapour cushion beneath its bottom (Figure 4b, Figure S7 and Movie S7, Supporting Information). Therefore, the interaction between the droplet and smooth region

corresponds to the film-boiling state. Many published studies have shown that enhanced hydrophilicity or surface nanoporosity can increase the Leidenfrost temperature, because rough surface micro/nanostructures can disturb the formation of a stable vapour layer.[45-47] The femtosecond laser-induced ripple microstructures not only increase the intrinsic hydrophilicity of the aluminium substrate as the CA decreases from 100.3° to 5.4° while introducing abundant nanoparticles and nanopores. Consequently, the Leidenfrost temperature (>600 °C) on the laser-structured surface is higher than that (200 °C on the untreated smooth aluminium sheet). When we used a small laser-scanning spacing to process the substrate and ensure full coverage of the aluminium surface by micro/nanostructures (eliminating untreated regions), the deposited droplets exhibited transition boiling characteristics on the resulting surface at a heating temperature of 250 °C (Figure S7 and Movie S7, Supporting Information). The bottom of the droplet contacts the heated surface, resulting in sustained contact boiling that causes many satellite droplets to scatter violently outwards. This result indicates that the droplet interacts with the heated laser-induced microstructures in the transition-boiling state (Figure 4c). Therefore, on a heated heterogeneous surface, the droplet experiences a hybrid boiling state: film boiling over smooth regions and transition boiling over ripple microstructures (Figure 4a).

The combined state allows the droplets to integrate the advantages of both the film- and transition-boiling states on the hot surface. The film-boiling state between the droplet and smooth region helps form a stable vapour layer between the droplet bottom and the solid substrate, approximately keeping the droplet in the Leidenfrost state on the heated sheet. The average thickness (δ) of the vapour layer can be estimated as $\delta \sim (\frac{k_v \Delta T_s \mu_v}{L \rho_v \rho_l g l_c})^{\frac{1}{4}} R^{\frac{1}{2}}$, where k_v is the thermal conductivity of the vapour, ΔT_s is the temperature difference between the heated substrate and the droplet bottom, μ_v is the viscosity of the vapour, L is the water latent heat of evaporation, ρ_v is the density of the vapour, g is the acceleration of gravity, $l_c \sim \sqrt{\gamma / \rho_l g}$ is the capillary length of the water, and R denotes the radius of the droplet.[1,3,40,48] For a droplet at the millimetre scale, the thickness of the vapour cushion is usually 10–100 μm, which is much greater than the undulation of the laser-induced craters.[1] The formation of a vapour cushion can significantly reduce the frictional resistance between the droplet and solid substrate, ensuring droplet motion. This vapour cushion also weakens the heat transfer from the heated surface to the droplet, thereby significantly prolonging the droplet's lifespan. The vapour layer also suppresses continuous contact between the droplet and laser-induced ripple microstructures, transforming the originally stable

liquid—solid contact into intermittent contact. Compared to the smooth regions, the laser-structured areas on the hot surface provide a bridge for rapid thermal energy transfer from the solid substrate to the bottom of the droplet through partial and local transition boiling contacts. Although only the peaks in the micro/nanostructures in the laser-treated region are allowed to intermittently contact the droplet bottom because of the existence of a vapour cushion, these contact points create transient hot spots at the bottom of the droplet (Figure 4c). The instantaneous localised boiling and rapid vapour evaporation at these hotspots generates the driving force for the directional motion of the droplet.[19,20,34]

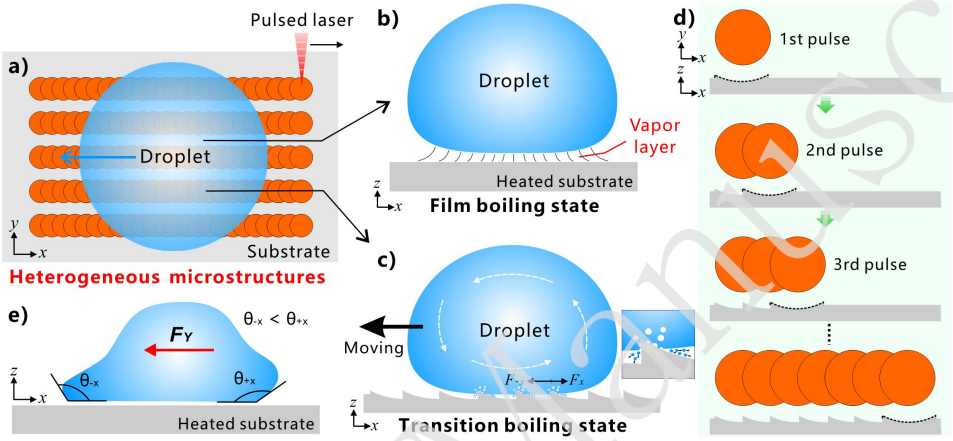

Figure 4. Mechanism of unidirectional self-propulsion of the Leidenfrost droplets on the laser-designed heterogeneous structures. (a) Schematic of a droplet on a heated heterogeneous surface. The bottom of the droplet simultaneously rests on both the non-ablated (untreated) smooth region and the laser-induced ripple microstructures. (b) Schematic of the droplet's state over the heated non-ablated smooth region. The droplet is in the film-boiling state, with a stable vapour layer formed between the droplet bottom and the heated substrate. (c) Schematic of the droplet's state over the heated ripple microstructures. The inset in (c) is an enlarged view of the boiling contact between the droplet bottom and a single peak of the ripple microstructure. During the intermittent contact between the bottom of the droplet and the peak parts of the ripple microstructures, the asymmetric ejection of vapour flow and tiny satellite droplets occurs violently at the localised hot spots on the droplet bottom. (d) Schematic of the formation process of periodic asymmetric ripple microstructures during femtosecond laser direct writing. The microscale ablation crater induced by the next laser pulse overlaps with the previous one, forming an overlapping microstructure along the laser-scanning line. (e) Schematic of the unbalanced Young's force generated by asymmetric CAs at both sides of a droplet.

To understand the mechanism by which laser-induced microstructures unidirectionally drive Leidenfrost droplets, understanding the formation of ripple microstructures during femtosecond laser direct writing is crucial. As shown in Figure 4d, when the first laser pulse irradiates the aluminium surface, a microscale concave crater is induced at the focal point. Because of material removal, the bottom of the crater lies below the horizontal plane of the substrate surface, whereas the edges

exhibit a slight protrusion caused by outwards material extrusion during laser interaction. This profile is typical of a single-pulse-induced crater structure.[49-51] As the laser focus moves forward, the second pulse arrives and is focused on the metal surface, with its position shifted relative to the previous ablation point. This step displacement (Λ_{crater}) is determined by both the repetition rate of the laser system and the scanning speed used during laser processing. The second pulse also produces a crater structure on the surface of the sample. By controlling the focal position to approximately overlap the edge of the first crater, the second laser-induced crater was superimposed on the first crater, covering half of the former crater. Similarly, the third pulse-induced crater overlaps with the second, covering half of it. This process repeats, resulting in a sequentially stacked microstructure, resembling overlapping fish scales, on the metal surface. Consequently, a periodic ripple-like microstructure forms along the laser-writing path (Figure 1e). As shown in Figure 4d, the highest point of each repeating unit (*i.e.,* the left protruding edge of a single-pulse-induced crater) exhibits an asymmetric profile on both sides. Along the laser-scanning direction, the profile of the right side of the highest point slopes gently downwards and belongs to the same crater as that of the highest point. In contrast, against the scanning direction, the left side of the highest point reveals a sharp step-down structure formed by the former partial crater.

Owing to the presence of a vapour layer underneath the droplet, the bottom of the droplet normally has difficulty in contacting the aluminium surface. However, because the droplet tends to bounce and oscillate on the heated surface and undergoes irregularly shaped oscillations, its bottom occasionally and intermittently contacts the elevated regions of the surface microstructures, *i.e.,* the peaks of the ripple microstructure. When the peaks of the ripples pierce the vapour layer and penetrate the droplet, intermittent hot spots form on the bottom surface of the droplet. The penetration of the surface microstructure peak into the liquid is substantiated by the formation of macroscopic bubbles within the droplet.[19,34] In these hotspot regions, partial contact boiling occurs, leading to intense local evaporation and the outwards ejection of tiny satellite droplets, as shown in Figure 4c. The high-speed jetting of the vapour and tiny satellite droplets can exert a recoil force ($\boldsymbol{F}_{recoil}$) on the droplet.[19,34] According to Newton's third law, the recoil force experienced by the droplet equals the rate of momentum change of the ejected material (including the vapour flow and tiny satellite droplets): $\boldsymbol{F}_{recoil} = -(\sum \dot{m}_v \boldsymbol{v}_v + \sum \dot{m}_l \boldsymbol{v}_l)$, where $\dot{m}_v$ and $\dot{m}_l$ are the mass ejection rates (mass ejected per unit time) of the vapour and tiny droplets, respectively, and $\boldsymbol{v}_v$ and $\boldsymbol{v}_l$ are the average ejection velocities of the vapour and

tiny droplets, respectively. During the process where the bottom of the droplet intermittently contacts and then rapidly detaches from the peaks of the ripple microstructures (*i.e.,* the intermittent contact process), an asymmetry arises: For a single ripple peak, the contact area between the droplet and the +*x* sloped side is larger than that of the -*x* stepped side, as shown in Figure 4c. Consequently, the heat transfer from the hot substrate to the droplet is more pronounced on the +*x* side at the hot spots, leading to more intense outwards vapour jets and tiny droplet ejections on that side. In other words, near the hot spots, the vapour and tiny satellite droplets ejected from the droplet's bottom in the +*x* direction are more vigorous, greater in volume, and faster in speed than those in the -*x* direction. Therefore, the recoil force acting on the droplet in the -*x* direction (F_{-x}) is stronger than that in the +*x* direction (F_{+x}), *i.e.,* $F_{-x} > F_{+x}$. Consequently, the intermittent contact between the droplet bottom and the laser-induced ripple microstructures subjects the droplet to an asymmetric momentum force.

However, laser-induced asymmetric surface microstructures can also lead to the asymmetric wettability of the material surface. Under ambient conditions, when a droplet is deposited onto a laser-structured surface, its spreading distance in the -*x* direction is greater than that in the +*x* direction; that is, the liquid exhibits preferential spreading along the -*x* direction (Figure S2 and Movie S1, Supporting Information). This asymmetric wettability results in different horizontal components of the surface tension across the droplet periphery, thereby generating an unbalanced Young's force (F_Y) along the horizontal direction, as shown in Figure 4e. The unbalanced Young's force acting on the droplet, derived via contact line integration, is given by: $F_Y = -\int_l \gamma(\cos\theta_{-x} - \cos\theta_{+x})\mathrm{d}l$, where l is the length of the solid-liquid contact line, and θ_{-x} and θ_{+x} are the CAs of the droplet along the –*x* and +*x* directions, respectively.[23,29,47,52] Owing to asymmetric spreading of the droplet, where $\theta_{-x} < \theta_{+x}$, the unbalanced Young's force F_Y would be along the -*x* direction. Consequently, both the recoil force caused by the outwards ejection of vapour and tiny satellite droplets and Young's force caused by the asymmetric wettability are dominant in the-*x* direction, driving the droplet to move directionally along the -*x* direction (opposite to the laser-scanning direction).

2.4 Diverse functions and applications based on directional droplet propulsion

Femtosecond laser processing is characterised by strong controllability, high flexibility, and wide applicability to various materials.[35-37,53-56] On heated heterogeneous surfaces, water droplets can be directionally driven at high speed along laser-scanning lines, with their movement direction opposite to that of laser processing. Because the laser-scanning path is precisely controlled via a programme,

the motion trajectory of Leidenfrost droplets can be easily designed by patterning laser-scanning lines, thereby enabling various functions and applications related to liquid propulsion under high-temperature conditions. For example, in most reported studies on self-propelled Leidenfrost droplets (such as those on ratchet structures), the droplets typically only move forward in a straight line, significantly limiting their potential applications owing to their lack of flexibility.[3,21-30] In contrast, with the femtosecond laser processing technique presented herein, the laser focus can follow curved scanning paths, allowing Leidenfrost droplets to be driven along curved and complex trajectories. On the surface shown in Figure 5a, we use a femtosecond laser to write a series of 'S'-shaped scanning lines on an aluminium surface. The water droplets deposited on the heated structured track are transported forward along the 'S'-shaped trajectory (Figure 5b and Movie S8, Supporting Information). If the laser-scanning lines are designed to extend from the outer edge of a circular region towards its centre, then the resulting structure exhibits droplet expulsion (Figure 5c). On the heated surface, irrespective of where the droplets are released onto the aluminium sheet, they are always driven outwards (away from the central region) and eventually exit the laser-treated zone (Figure 5d and Movie S8, Supporting Information). Conversely, when the laser-scanning lines are processed from the centre of the circular region to the outside, the designed pattern instead gathers the droplets towards the centre (Figure 5e). The droplets deposited on the heated surface spontaneously move inward (Figure 5f). This droplet-trapping structure can achieve targeted cooling of hot materials.[31,39] Upon placing a small piece of metal foam at the centre of the circular region, water droplets on the overheated substrate concentrate at the centre and are absorbed by the foam (Figure 5f and Movie S8, Supporting Information). Because of the rapid evaporation of the trapped water, the temperature of the central region drops, resulting in localised cooling. A 30-μL water droplet could reduce the central temperature from 270 °C to ≈200 °C (Figure 5g). Furthermore, if concentric circular scanning lines (Figure 5h) are written on the inner bottom of a mechanically machined circular concave pit (diameter = 34 mm, depth = 5 mm) on an aluminium block, then the droplets added to the concave pit rapidly rotate in a circular motion against the laser-scanning direction under heating (Figure 5i and Movie S8, Supporting Information). In this case, the droplet acts as a rotor, functioning similarly to a mini steam engine that converts thermal energy into mechanical energy. The Leidenfrost droplet rotor can potentially be used to drive other micromechanical devices.[26]

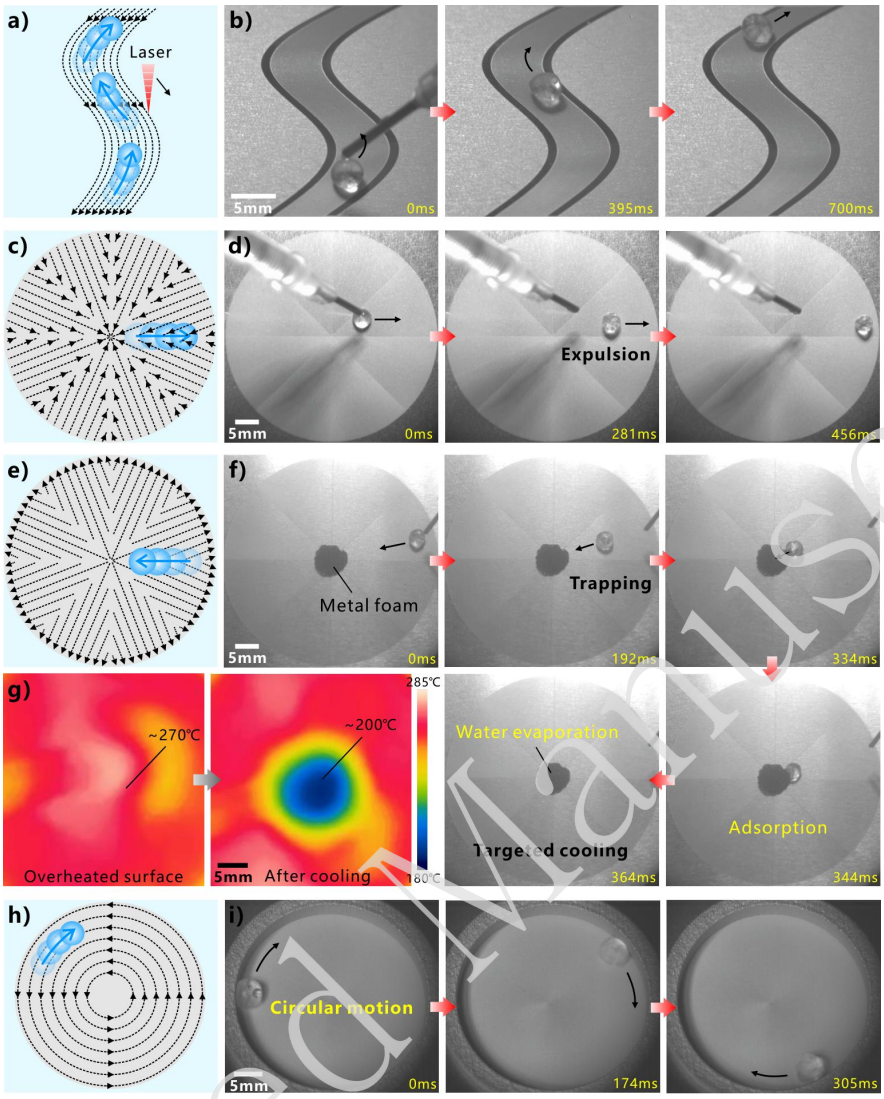

Figure 5. Multifunctional droplet propulsion and applications based on the structural design of the heated aluminium surface. (a,b) Driving a Leidenfrost droplet to transport along a curved ('S'-shaped) trajectory: (a) schematic of the patterned laser-scanning lines and (b) experimental snapshots of the droplet transport. (c,d) Droplet expulsion: (c) schematic of the patterned scanning lines and (d) process of a water droplet being transported outward. (e–g) Droplet trapping and localised cooling: (e) schematic of the patterned scanning lines, (f) process of a water droplet being transported inward, being absorbed by a metal foam, and rapid evaporation, and (g) infrared thermal images of the metal surface before and after droplet evaporation. (h, i) Leidenfrost droplet rotor: (h) schematic of the patterned scanning lines in the inner bottom of a circular concave pit and (i) process of droplet rotation in a circular motion. The black dashed lines with arrows in (a, c, e, h) denote the direction and path of laser processing.

3. Conclusions

In this study, a dual heterogeneous structure is designed on the surface of an

aluminium sheet via femtosecond laser direct writing. The surface is alternately covered by non-ablated smooth stripes and femtosecond-laser-structured regions, enabling droplets on the heated surface to be in the film-transition hybrid boiling state. The laser-treated areas consisted of periodic asymmetric ripple-like microstructures (η = 15.1–71.7%). On the heated sample surface with an appropriate heating temperature, whenever the bottom of a droplet intermittently contacts the peaks of these ripples, asymmetric and local contact boiling occurs at the hot spots, generating a directional driving force that propels the droplet overall in the Leidenfrost state to transport unidirectionally, with an adjustable velocity ranging from 24.3 to 129.9 mm/s. The Weber number (We = 6–34, representing the release height of the droplets) only negligibly influences the dynamic behaviour of the droplet on the laser-structured heterogeneous surface. Irrespective of the release height, the droplets undergo unidirectional transport uniformly at the same heating temperature. As the droplet volume increases from 7.0 μL to 31.1 μL, the critical temperature for transitioning from the boiling state to the unidirectional transport state gradually increases, whereas the volume variation negligibly affects the critical temperature for transitioning from the unidirectional transport state to the random motion state. The droplets on this heated heterogeneous surface exhibit the advantages of both the film- and transition-boiling states, achieving a balance between an extended lifespan and effective heat transfer. Interestingly, the droplets self-propel only along the laser-scanning lines and move in the direction opposite to that of laser processing. Precise control and design of the motion of Leidenfrost droplets on heated surfaces can be easily achieved by the direct laser writing of patterned scanning lines. Various intriguing functions and applications based on the controllable propulsion of Leidenfrost droplets have been realised, including curved-path droplet transport, droplet expulsion, droplet trapping, targeted cooling, and droplet rotors. The study of droplet dynamics on such heterogeneous heated surfaces not only enhances the fundamental understanding of the Leidenfrost effect but also paves the way for new engineering applications.

4. Experimental Section

4.1 Femtosecond laser processing

Because of their excellent thermal conductivity, (1060) aluminium sheets with a thickness of 1 mm were used as substrate materials. The laser beam (pulse duration = 35 fs, central wavelength = 800 nm, repetition rate = 1 kHz) generated from a femtosecond laser device (Spectra Physics) was focused onto the aluminium surface through a high-speed galvanometer scanner (S-9210D, Sunny Technology) and an f-θ

lens (focal length = 100 mm) with a spot diameter of ≈30 μm. The aluminium surfaces were ablated at a constant laser power of 350 mW (with a single-pulse energy of 350 μJ). The laser-scanning speed and interval of the scanning lines were adjusted to design the positional relationship between the laser-induced craters. The laser-scanning paths were controlled using a computer program.

4.2 Characterisation

The morphologies of the structured aluminium surfaces were observed using a scanning electron microscope (GeminiSEM 500, Carl Zeiss) and a laser confocal microscope (LSM900, Zeiss). The aluminium sheets were then heated using a heating plate (NH-R, Jiulian Tech. Co., Ltd.) at various temperatures. The heating temperature was monitored using a thermocouple embedded in a stainless-steel heating plate. The samples were carefully levelled before heating and testing. The motion of the droplet on the heated aluminium surface was recorded using a high-speed camera (Chronos 2.1-HD, Kron Technologies) at 1000 fps. The position and motion velocity of the droplets were obtained by analysing the recorded videos using MATLAB software. The temperature distribution on the metal sheet surface was captured using an infrared thermal imager (H21ProS+, HIKMICRO).

Supporting Information

Supporting Information is available from the author.

Conflicts of interest

There are no conflicts to declare.

Acknowledgement

This work was supported by the National Key Research and Development Program of China (No. 2024YFB4610700), the National Natural Science Foundation of China (Nos. 62475251, 62325507, 52305319, and 52206223), Fundamental Research Funds for the Central Universities (No. WK2090000088), and Xiaomi Young Scholars Program. We thank the Experimental Center of Engineering and Material Sciences at USTC for the fabrication and measurement of the samples. This work was partly carried out at the USTC Center for Micro- and Nanoscale Research and Fabrication and USTC Instruments Center for Physical Science.

References:

1. Gu, H. et al. Leidenfrost effect on engineered surfaces. *Advanced Functional Materials* **36**, 2423686 (2026).
2. Stewart, S. M. Leidenfrost drop dynamics: a forgotten past and modern day rediscoveries. *European Journal of Physics* **43**, 023001 (2022).
3. Wang, G. Q. et al. From thermal energy to kinetic energy: droplet motion triggered by the Leidenfrost effect. *Advanced Materials Interfaces* **8**, 2001249 (2021).
4. Quéré, D. Leidenfrost dynamics. *Annual Review of Fluid Mechanics* **45**, 197-215 (2013).
5. Biance, A. L., Clanet, C. & Quéré, D. Leidenfrost drops. *Physics of Fluids* **15**, 1632-1637 (2003).
6. Jiang, M. N. et al. Inhibiting the Leidenfrost effect above 1,000 °C for sustained thermal cooling. *Nature* **601**, 568-572 (2022).
7. Guo, Y. H. et al. Delayed Leidenfrost effect of a cutting droplet on a microgrooved tool surface. *Langmuir* **39**, 9648-9659 (2023).
8. Hai, A. et al. High-temperature wettable water-based lubricants toward hot rolling lubrication. *Advanced Functional Materials* **34**, 2316793 (2024).
9. Bouillant, A. et al. Leidenfrost wheels. *Nature Physics* **14**, 1188-1192 (2018).
10. Soto, D. et al. Air-levitated platelets: from take off to motion. *Journal of Fluid Mechanics* **814**, 535-546 (2017).
11. Yang, J. L. et al. A standing Leidenfrost drop with Sufi whirling. *Proceedings of the National Academy of Sciences of the United States of America* **120**, e2305567120 (2023).
12. Bain, R. M. et al. Accelerated chemical reactions and organic synthesis in Leidenfrost droplets. *Angewandte Chemie International Edition* **55**, 10478-10482 (2016).
13. Song, J. et al. Partial Leidenfrost evaporation-assisted ultrasensitive surface-enhanced Raman spectroscopy in a Janus water droplet on hierarchical plasmonic micro-/nanostructures. *ACS Nano* **14**, 9521-9531 (2020).
14. Liu, M. J. et al. Leidenfrost effect-induced chaotic vortex flow for efficient mixing of highly viscous droplets. *Advanced Materials* **36**, 2409192 (2024).
15. Vakarelski, I. U. et al. Stabilization of Leidenfrost vapour layer by textured superhydrophobic surfaces. *Nature* **489**, 274-277 (2012).
16. Wells, G. G. et al. A sublimation heat engine. *Nature Communications* **6**, 6390 (2015).
17. Liu, Y. et al. Femtosecond laser-produced heterogeneous wettability

surfaces for turning Leidenfrost drop spinning. *Applied Physics Letters* **125**, 071602 (2024).
18. Guo, Y. H. et al. Suppressed Leidenfrost effect on the rough tool surface with negative skewness for high-efficiency evaporation cooling. *Applied Thermal Engineering* **242**, 122445 (2024).
19. Guo, Y. H. et al. Singular ratchet-valley structure inducing droplet directional transport crossing all boiling states. *International Journal of Heat and Mass Transfer* **245**, 127005 (2025).
20. Jiao, Y. L. et al. Achieving the bidirectional transportation of boiling droplets on the functional ratchet-valley array. *Langmuir* **41**, 25315-25325 (2025).
21. Linke, H. et al. Self-propelled Leidenfrost droplets. *Physical Review Letters* **96**, 154502 (2006).
22. Lagubeau, G. et al. Leidenfrost on a ratchet. *Nature Physics* **7**, 395-398 (2011).
23. Liu, C. C. et al. Directional drop transport achieved on high-temperature anisotropic wetting surfaces. *Advanced Materials* **26**, 6086-6091 (2014).
24. Li, J. et al. Rectification of mobile Leidenfrost droplets by planar ratchets. *Small* **16**, 1901751 (2020).
25. Soto, D. et al. Surfing on a herringbone. *Physics Review Fluids* **1**, 013902 (2016).
26. Li, A. et al. Tailoring vapor film beneath a Leidenfrost drop. *Nature Communications* **14**, 2646 (2023).
27. Kruse, C. et al. Self-propelled droplets on heated surfaces with angled self-assembled micro/nanostructures. *Microfluidics and Nanofluidics* **18**, 1417-1424 (2015).
28. Li, B. H. et al. Self-propelled Leidenfrost droplets on femtosecond-laser-induced surface with periodic hydrophobicity gradient. *International Journal of Extreme Manufacturing* **6**, 025502 (2024).
29. Li, J. et al. Directional transport of high-temperature Janus droplets mediated by structural topography. *Nature Physics* **12**, 606-612 (2016).
30. Leon, V. J. & Varanasi, K. K. Self-propulsion of boiling droplets on thin heated oil films. *Physical Review Letters* **127**, 074502 (2021).
31. Liu, M. J. et al. Inhibiting random droplet motion on hot surfaces by engineering symmetry-breaking Janus-mushroom structure. *Advanced Materials* **32**, 1907999 (2020).
32. Cheng, Z. L. et al. Designable and unidirectional motion of Leidenfrost droplets on heated asymmetric microgrooves written by femtosecond laser. *Applied Physics Letters* **124**, 061601 (2024).
33. Liu, C. et al. Droplet interactions with hot surfaces: boiling modes,

Leidenfrost temperature, dynamics, and applications. *Small* **21**, 2501592 (2025).
34. Sahoo, V. et al. Elongated bouncing and reduced contact time of a drop in the Janus state. *Langmuir* **34**, 10874-10879 (2018).
35. Yong, J. L. et al. Nature-inspired superwettability achieved by femtosecond lasers. *Ultrafast Science* **2022**, 9895418 (2022).
36. Gao, L., Zhang, Q. M. & Gu, M. Femtosecond laser micro/nano processing: from fundamental to applications. *International Journal of Extreme Manufacturing* **7**, 022010 (2025).
37. Lin, Z. Y. & Hong, M. H. Femtosecond laser precision engineering: from micron, submicron, to nanoscale. *Ultrafast Science* **2021**, 9783514 (2021).
38. Yong, J. L. & Wu, D. Bioinspired controlling the surface wettability of materials by femtosecond laser: current progress and challenges (invited). *Chinese Journal of Lasers* **51**, 0102002 (2024).
39. Liu, C. et al. Steerable drops on heated concentric microgroove arrays. *Nature Communications* **13**, 3141 (2022).
40. Marín, Á. G. et al. Capillary droplets on leidenfrost micro-ratchets. *Physics of Fluids* **24**, 122001 (2012).
41. Liu, C. et al. One-step process for dual-scale ratchets with enhanced mobility of leidenfrost droplets. *Journal of Colloid and Interface Science* **569**, 229-234 (2020).
42. Long, J. Y. et al. Superhydrophilicity to superhydrophobicity transition of picosecond laser microstructured aluminum in ambient air. *Journal of Colloid and Interface Science* **441**, 1-9 (2015).
43. Liu, C. et al. Multibioinspired JANUS membranes with spatial surface refreshment for enhanced fog collection. *Advanced Materials Interfaces* **8**, 2101212 (2021).
44. Guo, Q. M. et al. Directional propulsion of transition boiling droplets on high-temperature surfaces induced by tilted nanoforests with asymmetric wettability. *Surfaces and Interfaces* **56**, 105623 (2025).
45. Kim, H. et al. On the effect of surface roughness height, wettability, and nanoporosity on leidenfrost phenomena. *Applied Physics Letters* **98**, 083121 (2011).
46. Kruse, C. et al. Extraordinary shifts of the Leidenfrost temperature from multiscale micro/nanostructured surfaces. *Langmuir* **29**, 9798-9806 (2013).
47. Agapov, R. L. et al. Asymmetric wettability of nanostructures directs Leidenfrost droplets. *ACS Nano* **8**, 860-867 (2014).
48. Dupeux, G. et al. Viscous mechanism for Leidenfrost propulsion on a ratchet. *Europhysics Letters* **96**, 58001 (2011).

49. Ben-Yakar, A. et al. Thermal and fluid processes of a thin melt zone during femtosecond laser ablation of glass: the formation of rims by single laser pulses. *Journal of Physics D*: *Applied Physics* **40**, 1447-1459 (2007).
50. Yong, J. L. et al. Rapid fabrication of large-area concave microlens arrays on PDMS by a femtosecond laser. *ACS Applied Materials & Interfaces* **5**, 9382-9385 (2013).
51. Borowiec, A. et al. Transmission and scanning electron microscopy studies of single femtosecond- laser-pulse ablation of silicon. *Applied Physics A* **76**, 201-207 (2003).
52. Zhang, P. P. et al. Bioinspired self-propulsion of water droplets at the convergence of Janus-textured heated substrates. *Advanced Functional Materials* **29**, 1904535 (2019).
53. Yong, J. L. et al. Triboelectric “electrostatic tweezers” for manipulating droplets on lubricated slippery surfaces prepared by femtosecond laser processing. *International Journal of Extreme Manufacturing* **6**, 035002 (2024).
54. Wang, Y. C. et al. Glycerol-assisted grain modulation in femtosecond-laser-induced photochemical synthesis of patterned ZnO nanomaterials. *Light*: *Advanced Manufacturing* **6**, 7 (2025).
55. Huang, L. et al. Imaging/nonimaging microoptical elements and stereoscopic systems based on femtosecond laser direct writing. *Light*: *Advanced Manufacturing* **4**, 37 (2023).
56. Zhang, B., Yan, W. C. & Chen, F. Recent advances in femtosecond laser direct writing of three-dimensional periodic photonic structures in transparent materials. *Advanced Photonics* **7**, 034002 (2025).